Dalton Transactions

Accepted Manuscript

This is an *Accepted Manuscript*, which has been through the RSC Publishing peer review process and has been accepted for publication.

Accepted Manuscripts are published online shortly after acceptance, which is prior to technical editing, formatting and proof reading. This free service from RSC Publishing allows authors to make their results available to the community, in citable form, before publication of the edited article. This *Accepted Manuscript* will be replaced by the edited and formatted *Advance Article* as soon as this is available.

To cite this manuscript please use its permanent Digital Object Identifier (DOI®), which is identical for all formats of publication.

More information about *Accepted Manuscripts* can be found in the **Information for Authors**.

Please note that technical editing may introduce minor changes to the text and/or graphics contained in the manuscript submitted by the author(s) which may alter content, and that the standard **Terms & Conditions** and the **ethical guidelines** that apply to the journal are still applicable. In no event shall the RSC be held responsible for any errors or omissions in these *Accepted Manuscript* manuscripts or any consequences arising from the use of any information contained in them.

Carbohydrate Linked Organotin(IV) Complexes as Human Topoisomerase Iα Inhibitor and their Antiproliferative Effects Against Human Carcinoma Cell Line

Rais Ahmad Khan[a,b], Shipra Yadav [a], Zahid Hussain [c], Farukh Arjmand[a] and Sartaj Tabassum.[a]*

[a*] *Department of Chemistry, Aligarh Muslim University, Aligarh –202002, India.*

[b] *Department of Chemistry, King Saud University, Riyadh, KSA.*

[c] *Centre of Excellence in Biotechnology Research, KSU, Riyadh, KSA.*

Abstract

Dimethyltin(IV) complexes with ethanolamine (**1**) and biologically significant N–glycosides (**2** and **3**) were designed and synthesized. The structural elucidation of complexes **1–3** was done using elemental and spectroscopic methods; in addition, complex **1** was studied by single crystal X–ray diffraction studies. *In vitro* DNA binding profile of the complexes **2** and **3** was carried out by employing different biophysical methods to ascertain the feasibility of glycosylated complexes. Further, the cleaving ability of **2** and **3** was investigated by agarose gel electrophoretic mobility assay with supercoiled pBR322 DNA, demonstrated significantly good nuclease activity. Furthermore, both the complexes exhibited significant inhibitory effects on the catalytic activity of human Topo I at lower concentration than standard drugs. The computer–aided molecular docking techniques were carried out to ascertain the mode and mechanism of action towards the molecular target DNA and Topo I. The cytotoxicity of the **2** and **3** against human hepatoma cancer cells (Huh7) was evaluated, which revealed significant regression in cancerous cells as compared with the standard drug. The antiproliferative activity of **2** and **3** were tested against the human hepatoma cancer cells (Huh7), results manifested significantly good activity. Additionally, to validate remarkable antiproliferative activity of **2** and **3** complexes, specific regulatory genes expression (MMP–2 and TGF–β) was obtained by real time PCR.

*Author to whom correspondence is to be done.

Corresponding Author Tel. No. : +91 9358255791.

E-mail address: tsartaj62@yahoo.com.

Introduction

Medicinal applications of metal complexes can be traced back to ancient times[1] with precious metals like gold and silver but the development of cisplatin, *cis*–diamminedichloroplatinum(II) spurred research interest in chemotherapeutic use of metal complexes for the treatment of cancer. Cisplatin, antineoplastic activity was discovered serendipitously by Rosenberg[2] in 1969 and approved for the treatment of solid cancers worldwide[3] in 1978. Since then, a number of metal–based chemotherapeutic agents have been designed and tested for their biomedical applications. However, serious adverse effects, such as dose–limiting nephrotoxicity, peripheral neuropathy, asthenia, myelosuppression and ototoxicity are known.[4] The intrinsic and acquired drug resistance during treatment further limited the application of cisplatin.[5] These serious limitations have prompted the search for unconventional chemotherapeutic strategies.

An emerging research area with considerable potential is organometallic medicinal chemistry.[6] Organometallic compounds exhibit potent anticancer activity,[6,7] including compounds that selectively inhibit enzymes,[8,9] or used to label peptides or other biomolecules.[10] Organotin(IV) complexes have received considerable attention owing to their potent biocidal activities, industrial and agricultural applications.[11,12] In the past decade, a large number of organotin derivatives have been prepared and tested *in vitro* and *in vivo* against murine leukemia cell lines (P388 and L1210) and on a panel of human cancer cell lines of different histological origin.[12c] While the organotin moiety is crucial for cytotoxicity, the ligand design also plays a key role in transporting and addressing the molecule to the target.[11] Now it is generally accepted that organotin(IV) moieties, may bind to glycoproteins, or to cellular proteins, directly interact with DNA, causing cell death by apoptotic mechanisms.[13] The tin-based compounds exhibit substantial binding to the phosphodiester backbone of DNA, change the intracellular metabolism

of the phospholipids of the endoplasmic reticulum.[13e] Recently, J. A. Ferragut, S. Gomez-Ruiz, et al., demonstrated that the organotin(IV) complexes are not P-glycoprotein substrates which strongly suggests that they do not induce acquisition of the undesirable multi -drug resistant phenotypes associated with the overexpression of this protein.[14] This is a notable property, encouraging further investigations on the anticancer activities of these tin-based compounds in *in vivo* systems.

The role of ligands is of considerable importance in tuning the cytotoxic characteristics of the complex. Ligands can modify the reactivity, lipophilicity, oral/systematic bioavailability of metal ions, stabilization of the oxidation state and substitutional inertness depending on the requirements for chemotherapy.[5,16] Among these carbohydrates represent an excellent class of tunable ligands for use in medicinal inorganic chemistry, they are often inexpensive, available in enantiomerically pure form, naturally available and possess functional groups for modulation according to the desired properties.[16,17] Furthermore, the potential benefit of appending carbohydrate moiety to metal complex lies in the modulation of hydrophilicity or lipophilicity which not only affects the cellular uptake of the compounds but also helps in their facile transport at the molecular level.[16,18] They are also known to interfere with carbohydrate–protein interactions and can inhibit cell–cell recognition and adhesion phenomena, which are crucial in cancer growth and progression.[19] Moreover, there are several compounds in clinical use as anticancer agents or in advanced clinical stage having a sugar moiety, e.g., the DNA strand break–inducing compound bleomycin,[20] the alkylating agent glufosfamide,[21] and the DNA intercalator doxorubicin (trade name adriamycin).[22]

The aim of the present study was to investigate new N–glycoside organotin complexes for the development of chemotherapeutic agents for treating cancers. Since the synthetic approach to

attach a bioactive ligand moiety to metal complexes has proven promising for developing efficacious drug entities and keeping in mind the various biological properties of carbohydrates, we have designed and synthesized the organotin(IV) complexes with ethanolamine (complex **1**) and N–glycosides (complexes **2** and **3**) and studied their interactions with CT DNA by employing various biophysical techniques. The *in vitro* DNA binding, nuclease activity, and Topo I inhibition activity showed capability of the complexes **2** and **3** of recognizing a specific sequence in DNA groove to inhibit the expression of Topo I *via* endolytic DNA cleavage process and thereby, control the replication of tumor cells. It is indeed gratifying to note that complexes **2** and **3** exhibited all the pre–requirements for efficient chemotherapeutic drug design which include increased bio–activity due to multi–faceted binding modes (tin as an apoptotic director), cleaving DNA, potent Topo I inhibitor activity and significantly good antiproliferative activity.

Results and discussion

The N–glycoside ligand was synthesized through condensation of D–glucose (**2**) and D–maltose (**3**) with ethanolamine using a similar method to that described earlier.[23–25] The corresponding complexes **2** and **3** were prepared by a direct reaction of the N–glycosidic ligands, with dimethyltin(IV) chloride in methanol as reported earlier by our group with slight modifications.[25] The outline of the synthetic procedure of the ligands and its organotin(IV) complex are presented in Scheme 1.

These complexes **1**–**3** were characterized by spectral studies using IR, NMR (^{1}H, ^{13}C and ^{119}Sn), ESI–MS and elemental analysis. The products were isolated as yellow solids. In addition to characterization by standard analytical methods, single crystal of the representative complex **1** was analyzed by X–ray diffraction.

Spectroscopic Studies

The FT IR spectrum of the complex **1** exhibited band of $\delta(NH_2)$ of the ethanolamine ligand at 1617 cm^{-1} and the appearance of signal at 472 cm^{-1} attributed to υ(Sn–O), which validated the coordination of ethanolamine *via* oxygen atoms with organotin(IV) metal core. Furthermore, infrared (FT IR) spectra of carbohydrate conjugate organotin(IV) complexes **2** and **3**, displayed merged and broadened characteristic bands of υ(O–H) due to hydrogen bonding in carbohydrate moieties in the range 3372–3356 cm^{-1}. A moderate band at ca. 1631–1628 cm^{-1} was assigned to δ(N–H) vibration of the glycosidic ligand.[24] The far IR spectra revealed absorption at ca. 440–433 cm^{-1} attributed to υ(Sn–O) vibration,[26] which confirmed the bonding of the oxygen atom of the N–glycoside ligand to the tin metal center.

The multinuclear (^1H, ^{13}C and ^{119}Sn) acquired in DMSO (**1**)/D_2O (**2** and **3**) showed functional group signatures as expected. In the ^1H NMR spectrum of complex **3** exhibited two doublets for two protons of each –OCHO– and –OCHN– at 5.37 and 5.19 ppm, respectively. A broad peak was found at 4.65 ppm associated with NH_2 protons of complex **1**. The characteristic skeletal protons of the N–glycoside moieties were obtained as multiplets around 3.99–3.02 ppm, for complexes **2** and **3**. The ^1H NMR spectra of the complexes **1**–**3** revealed singlet signals at 0.82–0.75 ppm attributed to the protons associated with the two methyl groups attached to Sn(IV) metal core. The ^1H NMR chemical shift assignment of the dimethyl tin moiety can be estimated from the multiplicity pattern and the ^2J [^{119}Sn, ^1H] coupling constant values. The dihedral C–Sn–C angles were calculated by applying Lockhart's equation (I).[27]

$$\theta = (0.0161)\,(^2J)^2 - (1.32)\,(^2J) + 133.4 \qquad \text{(I)}$$

The ^2J[^{119}Sn,^1H] coupling constant values of the complexes **1**–**3** were found to be 101.4, 101.8 and 102.1 Hz, respectively. The dihedral C–Sn–C angles were found to be 165.1° for **1** which is in very close proximity with experimental value of 164.8° (crystallographic data), 165.8° for **2**

and 166.4° for **3**, all the results were consistent with hexacoordinated environment around the Sn atom.

The ^{13}C NMR spectra of the complexes **1**–**3** explicitly resolved the resonance of all the distinct carbon atoms. The characteristic peaks associated with sugar resonances were observed in the range of 98.00–60.77 ppm for monosaccharide moieties of the complexes **2** whereas ^{13}C NMR pattern of disaccharide moiety showed the signals around 100.49–52.64 ppm. The ^{13}C NMR spectra of all the complexes showed signals at ca. 58.0 and 41.8 ppm for **1**, 51.2 and 39.3 ppm for **2** and 49.4 and 37.3 ppm for **3**, attributed to the two linking C–atoms of the 2–hydroxy ethylamine based linker.[28] Since $^{1}J(^{119}\text{Sn}–^{13}\text{C})$ coupling can also be used for determination of C–Sn–C bond angle. The coupling constants for the complexes **1**–**3** were found to be $^{1}J(^{13}\text{C}–^{119}\text{Sn})$ = 1012 Hz, 1019 Hz and 1023 Hz, respectively. Thus, the C–Sn–C (θ) angle in solution is calculated by applying Lockhart's equation (II) was obtained as 165.5º, 166.1º and 166.5º, respectively.

$$\theta = [^{1}J(^{119}\text{Sn}–^{13}\text{C}) + 875] / 11.4 \qquad \text{(II)}$$

In all cases, the data revealed distorted octahedral tin center and validated the above findings. Furthermore, the ^{119}Sn NMR spectra of the complexes **1**–**3** displayed chemical shift signals at –225.1, –208.1 and –142.6 ppm, which further confirmed the octahedral geometry of Sn(IV) metal core.

Single crystal X –ray Crystallography

The ORTEP view of the structure of the organotin(IV) complex, **SnEA** (**1**), along with the atom numbering scheme, is shown in Figure 1. The crystallographic data are given in Table 1.The organotin(IV) complex **1**, crystallizes as a monoclinic crystal system with space group *Cc* (*Z* = 4). The coordination geometry around Sn(IV) is pseudo–octahedral, in which C1—Sn1—C2 =

164.8 (5)°; angle deviates markedly from the ideal value of 180°. The angles O2—Sn1—Cl1 and O1—Sn1—Cl2 are 177.2(5)° and 176.4(4)°, respectively. The angles C1–Sn1–O1, O1–Sn–O2, C1–Sn–Cl1 and C1–Sn–Cl2, were 86.7(6)°, 87.8(3)°, 97.8(6)° and 92.9(5)°, respectively deviate by around ±4–8° from the 90° expected for a perfect octahedral geometry. The Sn(IV) core was coordinated with two oxygen's (Sn1−O1, 2.339(14) Å; Sn1−SnO2, 2.385(13) Å), two chlorides (Sn1−Cl1, 2.491(5) Å; Sn1−Cl2, 2.496(6) Å) and two methyl groups (Sn1−C1, 2.09 (2) Å; Sn1−C2, 2.126 (18) Å).

***In vitro* DNA Binding Studies**

In understanding the mechanism of tumor inhibition for the treatment of cancer, DNA is the primary intracellular target of antitumor drugs, thus metallodrug–DNA interaction is of paramount importance. Coordination compounds offer many binding modes to polynucleotides, including outer–sphere non–covalent binding, metal coordination to nucleobases and phosphate backbone interactions. Therefore, in order to have an insight on the binding propensity and binding mode, interaction of complexes **1**–**3** with calf thymus DNA (CT DNA) was analyzed by using different biophysical techniques such as absorption and emission spectral studies.

Electronic absorption titration

Electronic absorption spectroscopy is one of the most common ways to investigate the interactions of complexes with DNA followed by the changes in the absorbance and shift in the wavelength. DNA binding ability of all the complexes **1**–**3** was evaluated by electronic absorption spectroscopy by studying metal complex–DNA interactions. In the UV region, the complexes **1**–**3**, exhibited intense absorption bands around 236–238 nm attributed to intraligand transitions. Fig. 2 illustrates the respective absorption spectral changes of complexes **2** and **3** in absence and presence of CT DNA.

Binding of the complexes to DNA is expected to perturb the ligand centered transitions of complexes. Upon the addition of increasing amounts (0.067–0.33 × 10^{-4} M) of CT DNA to complexes **1**–**3** of fixed concentration (0.067 × 10^{-4} M), there was an increase in the absorption intensity "hyperchromaticity" followed by concomitant red shift of 2–3 nm which arises due to the preferential binding of the pre–dissociated Sn(IV) to nucleotides *via*, phosphate groups of DNA. Since Lewis acidic Sn(IV) cation exhibit tendency to exchange their coordinated ligand on addition of electron donor atoms (solvent molecules) or by the coordination to the nucleotides.[29] Moreover, the affinity of Sn(IV) with negatively charged phosphate group is very strong because of its hard Lewis acidic property ,the intrinsic binding constant K_b values obtained for the complexes **1**–**3**, were of the order 2.4 x 10^4, 8.8 x 10^4, 16.0 x 10^4 M^{-1}, respectively with a mean standard deviation of ± 0.02. These K_b values were compared to the cisplatin and our observation revealed that K_b values of **2** and **3** were greater in magnitude to that of the cisplatin (5.73 ±0.45 x 10^4 M^{-1}) as reported in literature.[30] Furthermore, complexes **2** and **3** possess a sugar scaffold *viz*., N–glycoside, which is lipophilic in nature and encourage affinity for the DNA groove binding.[31] These results suggest that the complex **3** is more avid DNA binder as compared **2**. This can also attributed to the extra stabilization due to hydrogen bonding between –NH and –OH of N–glycosides with the functional groups positioned on the edge of DNA bases as it provides molecular recognition at the specific site of the cellular target.[32]

Luminescence studies

To further elucidate the mode of binding of organotin complexes **1**–**3** with CT DNA, fluorescence spectral methods were employed by following the changes in the emission intensity of the complexes. In absence of DNA, emit luminescence around 262 nm in Tris–HCl buffer pH 7.2 when excited at 238 nm. Fixed volume (1.0 x 10^{-4} M) of the studied complexes **1**–**3** was

titrated with increasing concentration of CT DNA in the range from (0–0.40 x 10^{-4} M), respectively. The enhancements in the emission intensity of **2** and **3** with increasing CT DNA concentration are depicted in Fig. 3.

The observed enhancement could be due to relatively non–polar environment of the bound metal complex in the presence of DNA, such that the complexes were less deeply inserted inside the hydrophobic pockets or grooves of CT DNA. Cationic complexes usually bind to DNA non–covalently as the cationic core of the complexes exerts a strong electrostatic attraction to the anionic phosphate backbone of DNA thus precluding substantial overlap with the base pairs leading to higher emission intensity indicative of electrostatic binding of the probe to the DNA. Sn(IV) complex interacts with the phosphate group of DNA, and cause the contraction and conformational change of DNA helix, due to the fact that phosphate group can provide the suitable anchors for coordination with Sn(IV) complexes and consequently results in breakage of the secondary structure of the DNA. However, the presence of carbohydrate in a drug is important in molecular recognition at the specific site of DNA and has profound effect on biological activity. This effect was first studied in a family of anthracycline antibiotics, [33] which showed that carbohydrate makes the van der Waal's contacts with the minor groove of the DNA. In addition to electrostatic interactions, other kinds of forces involving non–polar interactions between carbohydrates cannot be excluded.[34] Therefore, the above results indicate that complexes **2** and **3** may first bind with the phosphate group of DNA, neutralize the negative charge of DNA phosphate group, and cause the contraction and conformational change of DNA.

To quantify the extent of DNA binding, the intrinsic binding constant (K_b) of the complexes **1**–**3** were determined using Wolfe–Shimer equation.[35] The K_b values were found to be 1.1 x 10^3, 1.4 x 10^4, 2.5 x 10^4 M^{-1}, respectively.

Effect of phosphate group on the binding of complexes with CT DNA

To further investigate the selective binding site of the complexes **2** and **3** with CT DNA, the fluorescence titrations were performed in the presence of K_2HPO_4 at 25 ºC (Fig. 4).With increasing amount of K_2HPO_4, fluorescence intensity of the complexes **1**–**3** increase appreciably demonstrating a competitive binding behavior between the phosphate group of K_2HPO_4 and the phosphate component of DNA backbone.[34] Therefore, the phosphate group of K_2HPO_4 weakens the interaction between the complexes and DNA, this observation provides supportive evidence for electrostatic interaction of the complexes **1**–**3** which bind selectively to the phosphate group of DNA double helix.[36] However, the enhancement in the intensity of complexes followed the order **3** > **2** > **1**, can be attributed to increase in hydrophobicity of the complexes **1**–**3** because of the linked carbohydrate moieties. These observations provided supportive evidence for electrostatic interaction of the Sn(IV) complexes which exhibit selective binding to the phosphate group of DNA double helix. Furthermore, there is a strong evidence in literature for Sn(IV)–phosphate binding which is validated by binding studies of Sn(IV) complexes with nucleotides employing NMR techniques.[37]

Effect of ionic strength on the binding of complexes with CT DNA

Furthermore, to understand the binding mode between the molecule and DNA, fluorescence titrations were carried out under the conditions of increasing ionic strength through added amounts of NaCl. The fluorescence intensity of the studied complexes **1**–**3** was appreciably quenched with increasing ionic strength as depicted in Fig. 5.

These significant quenching in fluorescence intensity indicate that a cation *viz.,* Na^+ can bind to phosphate group of the DNA by electrostatic forces to form a cation atmosphere around DNA. The presence of cationic environment shields DNA and inhibits the binding of the positively

charged molecules to the DNA phosphate backbone. Moreover, this invokes a competitive interaction for the phosphate anions and subsequent addition of the cations weaken the surface binding interactions and hydrogen bonding between DNA and molecule. Therefore, the results implicate that the complexes **1**–**3** predominantly binds to DNA phosphate backbone by electrostatic interactions.[38]

DNA cleavage studies

There has been considerable interest in DNA endonucleolytic cleavage reactions that are activated by metal complexes.[39,40] To ascertain the ability of the complexes **2** and **3** to serve as potential metallonuclease, the DNA cleavage were performed with pBR322 DNA incubated with varying concentration of the complexes in 5mM Tris–HCl/50mM NaCl buffer at pH 7.2, for 1h by agarose gel electrophoresis.[41] Gel electrophoretic pattern of complexes **2** and **3** were obtained (Fig. 6a and b), due to their high binding ability for DNA as evidenced by UV, fluorescence studies. Initially in the untreated pBR322 plasmid DNA (control, Lane 1) one band corresponding to Form I (supercoiled form) was observed. When the supercoiled pBR322 plasmid DNA were treated with the 10 μM of both the complexes **2** and **3**, the supercoiled DNA (Form I) was cleaved to nicked circular DNA (Form II) without the appearance of linear DNA form (Form III) (Lanes 2 and 3), respectively. With increasing concentration of the complexes **2** and **3** from 20–50 μM, obtained characteristic patterns for Sn(IV) complexes *viz.,* the appearance of faded bands and provides a measure of the extent of hydrolysis of the phosphodiester bond of DNA. Furthermore in complex **2**, adduct formation is made discernible by the EthBr (used to stain DNA) bound to it at a concentration of 20 μM but on further increase in concentration, formation of adduct was reduced to a significant extent.

Human Topo I inhibition

Topoisomerases are over–expressed in many types of cancers and thus are major targets for antineoplastic agents such as doxorubicin, etoposide, and mitoxantrone.[42,43] Topoisomerases are isomerase enzymes that change the topology of DNA by introducing a transient break in the DNA strand, allowing a second DNA region from either the same molecule (relaxation, knotting, or unknotting) or a different molecule (catenation or decatenation) to pass through. During this process, the enzymes are covalently bound to the DNA *via* an active tyrosine residue, termed "cleavable complex". After the DNA is untangled or unwound, the strands are reannealed by the enzyme so that the overall composition of the DNA strand does not change. DNA topoisomerases are participating in nearly all biological processes involving DNA including replication, transcription, recombination, and chromatin remodeling.[44,45] This DNA–damaging effect, outside of its potentially curative properties, may lead to secondary neoplasms in the patient. Thus, DNA cleavage assay was used to investigate the effect of complexes **2** and **3** on the activity of human Topo I by agarose gel electrophoresis. This assay provides a direct means of determining whether the drug affects the unwinding of a supercoiled (SC) duplex DNA to nicked open circular (NOC) and relaxed (R) DNA. The activity pattern showed significant inhibition in a concentration–dependent manner.

As shown in Fig. 7, upon increasing the concentration of complexes **2** and **3** (20–40 μM), the levels of relaxed form were inhibited (lanes 3–6). At 40 μM the DNA relaxation effect caused by Topo I was completely inhibited by complex **2** whereas about 90% inhibition was perceived by **3**. The Topo I inhibitory activity of complexes **2** and **3** was significantly higher than some of the classical Topo I inhibitors used as antitumor drugs in clinic (Table 2).[46–48]

MTT Assay

The in vitro cytotoxicity assay for complexes **2** and **3** was assessed using the method of MTT reduction. Cisplatin was used as a positive control. After treatment of human hepatoma cancer cells (Huh7) for 48 h with complexes **2** and **3**, in the range of concentration (0-50 μM). The inhibitory percentage against growth of cancer cells was determined. The cell viability (%) obtained with continuous exposure for 48 h are depicted in Fig. 8. The cytotoxicity of complexes was found to be concentration-dependent. The cell viability decreased with increasing the concentrations of complexes **2** and **3**. The IC_{50} value was ~30-35 μM for both the complexes.

Antiproliferative activity

The growth–inhibitory effect of complexes **2** and **3** was examined on human hepatoma cancer cells (Huh7). The complexes were analyzed for the antiproliferative activity and expression of different genes involved in cancer. To test *in vitro* antiproliferative effect of **2** and **3** on hepatocellular carcinoma cell lines (Huh7), treatment dose was optimized to avoid cell cytotoxicity. Huh7 cells were seeded at the same density and subjected to optimum dose of this compound along with control in six well plates. The optimized dose was used to treat at 0 h and antiproliferative effect was analyzed at different time 0, 24 and 48h (Fig. 9). The complexes **2** and **3** significantly reduce the cell doubling time as well it showed limited cytotoxicity. Thus, our antiproliferative data confirmed the role of complexes **2** and **3** in reducing the cell doubling time and hence proliferation.

Expression of MMP–2 and TGF–β by real time PCR

To get further insight on significantly good antiproliferative activity complexes **2** and **3**, the level of expression of MMP–2 and TGF–β was measured by real time PCR.

Effect on tumor promoting MMP–2 gene

Tumor cell invasion and metastasis involve multiple steps, including proteolytic degradation of the basement membrane and extracellular matrix, altered cell adhesion and the physical movement of tumor cells. The excessive degradation of the matrix is one of the hallmarks of tumor invasion and metastasis.[49] Matrix metalloproteinases (MMPs) belong to important family of proteolytic enzymes involved in extracellular matrix degradation. Several studies have reported a positive correlation between MMP–2 and invasion of malignant tumors.[50–52] Therefore we have tested and analyzed complexes **2** and **3** on the transcriptional regulation of MMP–2. The cells treated with optimized concentration of complexes **2** and **3**, along with vehicle control only were subjected to total cellular RNA isolation. The total cellular RNA was collected and analyzed for the expression of MMP–2 mRNA levels. Our results indicated that Huh7 cells treated with complexes **2** and **3** significantly reduce the expression of MMP–2 mRNA levels (Fig. 10a). These findings establish that the carbohydrate–conjugate organotin complexes **2** and **3** have antiproliferative and anticancer effects. However, the effect of complex **2** is slightly higher in comparison to **3,** may be attributed to the more significant role of monosaccharides compared to disaccharide moieties associated with the complexes.

Effect on transforming growth factor–β (TGF–β)

Transforming growth factor–β (TGF–β) is a pleiotropic cytokine that regulates cell proliferation, angiogenesis, metastasis, and immune suppression.[53–55] TGF–β has biphasic effect in tumor growth; carcinogenesis and early tumor growth are suppressed by TGF–β whereas this growth factor apparently accelerates tumor progression in more advanced aggressive tumors.[51,52] Therefore, we have investigated how complex **2** and **3** effect the mRNA expression in hepatocellular carcinoma cell line. We found that both complexes do not have significant effect on the enhancement of the mRNA expression of TGF–β (Fig. 10b). The results of expression of

MMP–2 and TGF–β obtained by real time PCR recommends the involvement of MMP–2 gene in the antiproliferative effect.

Molecular Docking

Molecular docking with DNA

Molecular docking technique is an attractive scaffold to understand the Drug–DNA interactions in rational drug design, as well as in the mechanistic study by placing molecule into the binding site of the target specific region of the DNA mainly in a non–covalent fashion and to predict the correct binding mode and binding affinities.[56] Targeting the minor groove of DNA through binding to a small molecule has long been considered an important tool in molecular recognition of a specific DNA–sequence.[57] In our experiment, rigid molecular docking studies of complexes **2** and **3** with DNA duplex of sequence d(CGCGAATTCGCG)$_2$ dodecamer (PDB ID: 1BNA) were performed in order to predict the chosen binding site along with preferred orientation of the chemical species inside the DNA minor groove. The minimum energy docked pose (Fig. 11) revealed that complexes snuggly fitted into the curve contour of the targeted DNA in the minor groove, within G–C (~13.2 A) region, which slightly bends the DNA in such a way that the saccharine moiety makes favorable van der Waals interaction and hydrophobic contacts with DNA functional groups that define the stability of groove. Moreover, –OH groups of the complexes acts as strong H–bond donor or acceptor and were engaged in hydrogen–bonding interactions with DNA nucleobases available in the minor grooves. The resulting relative binding energy of docked complexes **2** and **3** with DNA were found to be –272.4 and –324.3 KJ mol^{-1} respectively, correlating well with the experimental DNA binding values. Thus, we can conclude that there is a mutual complement between spectroscopic studies and molecular docking

techniques, which can substantiate our experimental results and at the same time provides further evidence of groove binding.

Molecular docking with topoisomerase–I

To study the molecular basis of interaction and rationalize the observed enzymatic activity, molecular docking studies of complexes **2** and **3** with Topo I were carried out to search the exact binding site. The X–ray crystallographic structure of the human–DNA–Topo I complex (PDB ID: 1SC7) revealed that the Topo I is bound to oligonucleotide sequence 5′–AAAAAGACTTsX–GAAAATTTTT–3′, where 's' is 5′–bridging phosphorothiolate of the cleaved strand and 'X' represents any of the four bases A, G, C or T. The phosphoester bond of G12 in 1SC7 was rebuilt and SH of G11 on the scissile strand was changed to OH.[58] The analysis of best docked conformation (Fig. 11) revealed that both complexes **2** and **3** approaches towards the DNA cleavage site in the DNA–topo I complex and forming a stable complex through π–π stacking interactions between the G11 (+1) and pyrimidine ring of T10 (–1) in the minor groove on the scissile strand at C112 and A113, on the non–scissile strand, parallel to the plane of base pairs without having hydrogen bonds with the enzyme, subsequently leading to inhibitory effect on Topo I.[59]

The insertion of complexes between the DNA base pairs at the cleavage site results in increased physical distance between the cleaved DNA termini and consequently inhibition of the religation step catalyzed by Topo I. The resulting relative binding energy of Topo I docked complexes **2** and **3** were found to be –322.8 and –353.3 KJ mol^{-1} respectively, which revealed efficient binding of the complexes. Thus, computer–aided molecular docking studies afford valuable information of drug binding mode in the active site of DNA–topo I leading to the rational design of new classes of anticancer drugs targeting Topo I.

Experimental section

Materials and Methods

Glucose, maltose, dimethyltin dichloride, disodium salt of calf thymus DNA (highly polymerized stored at 4 ºC), agarose, (Sigma–Aldrich), ethanolamine, Tris(hydroxymethyl)aminomethane (E. Merck), and supercoiled pBR322 DNA (Genei) were used as received. Microanalysis (C, H and N) were carried out with a Carlo Erba Analyzer Model 1108. Molar conductances were measured at room temperature on a Eutech CON 510 conductivity bridge. Interspec 2020 FTIR spectrometer was used for recording IR spectra of KBr pellets in the range of 4000–400 cm^{-1}. Specific rotation was measured on a JASCO P–1020 (Jasco International Co., Ltd., Tokyo, Japan) digital polarimeter with a 10 cm optical length cell at 25 °C. ^{1}H, ^{13}C and ^{119}Sn NMR were recorded on Bruker Avance II 400 NMR spectrometer at 25 ºC. The collected data were reduced by using the program SAINT,[60] and empirical absorption corrections were done using the SADABS.[61]The structure was solved by direct methods and refined with the full–matrix least squares techniques using SHELX–97.[62] The positions of all atoms were obtained by direct methods. Anisotropic thermal parameters were assigned to all non–hydrogen atoms and the remaining hydrogen atoms were placed in geometrically constrained positions and refined as riding atoms with a common fixed isotropic thermal parameter. ORTEP 3 was used to produce graphical representation.[63]

Electronic spectra were recorded on UV–1700 PharmaSpec UV–vis spectrophotometer (Shimadzu). Electrospray mass spectra were recorded on Micromass Quattro II triple quadrupol mass spectrometer. Emission spectra were determined with a Shimadzu RF 5301 PC spectrofluorophotometer. Cleavage experiments were performed with the help of Axygen

electrophoresis supported by Genei power supply with a potential range of 50–500 Volts, visualized and photographed by Vilber–INFINITY gel documentation system.

Synthesis and characterization

Synthesis of SnEA complex (1)

To a solution of dimethyltin(IV) dichloride (0.219 g, 1 mmol) in dry dichloromethane (10 mL) was added ethanolamine (0.12 mL, 2 mmol) drop wise and allowed to stir for 2h and then filtered. The filtrate was kept for evaporation at room temperature and crystalline material was formed, which was filtered, washed with hexane and ether, and dried in vacuo. Recrystallisation in dry ethanol gives rise to colorless single crystals. Yield: 0.30 g, 89 %; m.p. = decompose at 300 ºC; anal. calc. for $C_6H_{20}Cl_2N_2O_2Sn$ (341.7): C 21.07; H 5.90; N 8.19; found: C 21.20; H 5.32; N 8.23; ESI–MS *m/z* {in DMSO, calcd (observed)} for $[C_6H_{20}Cl_2N_2O_2Sn]$: 341.7 (341.7); FT IR (KBr pellets) cm^{-1}: 1617 $\delta(NH_2)$; 472 υ(Sn–O); ^{1}H NMR (400MHz, DMSO, ppm): 4.65 (br, $–NH_2$, 4H), 3.77-3.69 (m, $HO\underline{C}H_2$, 4H), 2.90-2.84 (m, $\underline{C}H_2NH_2$, 4H), 0.82 (s, CH_3, 6H [$^2J(^{119}Sn–^1H)$ = 101.4 Hz, $^2J(^{117}Sn–^1H)$ = 99.2 Hz, $SnCH_3$)]; ^{13}C NMR (100MHz, DMSO, ppm): 58.0($\underline{C}H_2$–O), 41.8($\underline{C}H_2$–N), 15.3($\underline{C}H_3Sn$) [$^1J(^{119}Sn–^{13}C)$ = 1012 Hz, $^1J(^{117}Sn–^{13}C)$ = 1009 Hz, $SnCH_3$)]. ^{119}Sn NMR (149MHz, DMSO, ppm): –225.1.

Synthesis of GSnEA complex (2)

To a methanolic solution (10 mL) of N–glycoside synthesized by a reaction between D–glucose (0.360 g, 2 mmol) and ethanolamine (0.12 mL, 2 mmol) in methanol at 60 ºC for 1h, was added dimethyltin(IV)dichloride (0.219 g, 1 mmol) in dry ethanol (5 mL) drop wise and allowed to stir for 4h. Light brown color product was obtained, washed with hexane and ether, and dried in vacuo. Yield: 0.39 g, 58%; m.p. = hygroscopic. $[\alpha]_D^{25}$ = +58.6 (10^{-3} M, H_2O). Anal. calc. for $C_{18}H_{40}Cl_2N_2O_{12}Sn$ (665.9): C 32.44; H 6.05; N 4.21; found: C 32.49; H 5.75; N 4.21. ESI–MS

m/z {in H_2O, calcd (observed)} for [$C_{18}H_{40}Cl_2N_2O_{12}Sn$ + $2H^+$]: 667.9 (667.9). FT IR (KBr pellets) cm^{-1}: 3372 br, υ(OH); 1631 δ(N–H of N–glycoside); 1450 δ(OCH, CH_2, CCH); 1336, 1019 υ(CO); 1062 υ(CO, CC); 434 υ(Sn–O); ^{1}H NMR (400MHz, D_2O, ppm): 3.99–3.02 (m, –CH_2, –CH, –OCHC–, –NCHC–, OH, NH, 24H), 1.44–1.40 (m, CH_2, 4H), 1.26–1.21 (m, CH_2, 4H), 0.77 (s, CH_3, 6H) [^2J(^{119}Sn–^{1}H) = 101.8 Hz [^2J(^{117}Sn–^{1}H) = 98.0 Hz, $SnCH_3$)]; ^{13}C NMR (100MHz, D_2O, ppm): 98.0 (C1), 87.8 (C2), 80.6(C3), 75.9, 74.4(C5), 71.2, 69.6(C4), 62.5, 61.5 (C6, $\underline{C}H_2OH$ of sugar moiety), 60.8 ($\underline{C}H_2$–O, linker), 33.3($\underline{C}H_2$–N, linker), 13.0($\underline{C}H_3Sn$) [^1J(^{119}Sn–^{13}C) = 1019 Hz, ^1J(^{117}Sn–^{13}C) = 1017 Hz, $SnCH_3$)]. ^{119}Sn NMR (149 MHz, D_2O, ppm): –208.1.

Synthesis of MSnEA complex (3)

This complex was prepared from D–maltose (0.684 g, 2 mmol). According to the procedure described above for complex **2**. Light brown color product was obtained, washed with hexane and ether, and dried in vacuo. Yield: 0.52 g, 53 %; m.p. = hygroscopic. $[\alpha]_D^{25}$ = + 143.2 (10^{-3} M, H_2O); anal. calc. for $C_{30}H_{60}Cl_2N_2O_{22}Sn$ (990.0): C 36.36; H 6.11; N 2.83; found: C 36.40; H 5.88; N 2.81. ESI–MS *m/z* {in H_2O, calcd (observed)} for [$C_{30}H_{60}Cl_2N_2O_{22}Sn$ + $2H^+$]: 992.0 (991.5). FT IR (KBr pellets) cm^{-1}: br, 3356 (OH), 1628 [δ(N–H of N –glycoside)], 1441 [δ(OCH, CH_2, CCH)], 1334, 1016 [υ(CO)], 1068 [υ(CO, CC)], 440 [υ(Sn–O)]. ^{1}H NMR (400MHz, D_2O, ppm): 5.37–5.36 (d, –OCHO–, 2H), 5.19–5.18 (d, –OCHN–, 2H), 3.98 –3.08 (m, –CH_2, –CH, –OCHC–, –NCHC–, OH, NH, 32H), 1.48–1.46 (m, CH_2, 4H), 1.31–1.29 (m, CH_2, 4H), 0.71 (s, CH_3, 6H) [^2J(^{119}Sn–^{1}H) = 102.1 Hz, ^2J(^{117}Sn–^{1}H) = 98.8 Hz, $SnCH_3$)]; ^{13}C NMR (100MHz, D_2O, ppm): 100.5 (C1′), 97.7, 95.4 (C1), 82.2 (C3), 74.0 (C5), 72.7 (C4), 72.3 (C2), 71.6(C2′), 70.9, 69.5 (C3′), 69.3, 68.7 (C5′), 63.9, 61.5 (C4′), 60.4(C4′), 57.5 (C6), 56.1

(C6′), 49.7 (<u>C</u>H_2–O, linker), 33.3 (<u>C</u>H_2–N, linker), 13.0 (<u>C</u>H_3Sn) [$^1J(^{119}Sn-^{13}C)$ = 1023 Hz, $^1J(^{117}Sn-^{13}C)$ = 1020 Hz, $SnCH_3$)]. ^{119}Sn NMR (149MHz, D_2O, ppm): –142.6.

DNA binding and cleavage studies

DNA binding experiments that include absorption spectral studies, fluorescence conformed to the standard methods[35,64,65] and practices previously adopted by our laboratory.[23,66] Standard error limits were estimated using all data points.

Cleavage experiments of supercoiled pBR322 DNA (300 ng) by the complexes **2** and **3** (5.0–25.0 μM) in (5mM Tris–HCl/50 mM NaCl), buffer at pH 7.2 were carried out by agarose gel electrophoresis. The samples were incubated for 1h at 37 °C. A loading buffer containing 25% bromophenol blue, 0.25% xylene cyanol, 30% glycerol was added and electrophoresis was carried out at 30 V for 3 h in Tris–HCl buffer using 1% agarose gel containing 1.0 μg/mL ethidium bromide (EthBr). The standard protocols were followed for these experiments.

Topoisomerase I inhibition assay

Human DNA topoisomerase I (Topo I) was purchased from CALBIOCHEM and no further purification was performed. One unit of the enzyme was defined as completely relax 1 μg of negatively supercoiled pBR322 DNA in 30 min at 37 ºC under the standard assay conditions. The reaction mixture (20 μL) contained 35 mM Tris–HCl (pH 8.0), 72 mM KCl, 5 mM $MgCl_2$, 5 mM DTT, 2 mM spermidine, 0.1 mg/mL BSA, 1 μg pBR322 DNA, 1 Unit Topo I and complexes. These reaction mixtures were incubated at 37 ºC for 30 min, and the reaction was terminated by addition of 4 μL of stock solution consisting of 0.25% bromophenol blue, 4.5% SDS and 45% glycerol. The samples were electrophoresed through 1% agarose in TBE at 30 V for 5h. The concentration of the inhibitor that prevented 50% of the supercoiled DNA from being

converted into relaxed DNA (IC_{50} values) was calculated by the midpoint concentration for drug–induced DNA unwinding.

MTT assay

For the study of cell viability, 5 x 10^3 cells were plated in each well of a flat-bottom 96-well culture plate and incubated for 24 h treatment to different concentration (0 - 50 μM of complex **2** and **3** for 48 h), the cells were treated with 10 mL 3-(4,5-di-methyithiazol-2-yl)-2,5-diphenyl-2H-tetrazolium bromide (MTT) and incubated for 3 h at 37° C in a humidified incubator containing 5% CO_2. To dissolve the cells, we used 100 mL of DMSO and measured the resulting solutions absorbance at 570 nm by microplate reader (Elisa Biotek). DMSO was used as the solvent control. Data were collected for duplicates and used to calculate the respective means. The percentage inhibition was calculated, from this data, using the formula:

$$\frac{\text{Mean absorbance of untreated cells (control)} - \text{Mean absorbance of treated cells} \times 100}{\text{Mean absorbance of untreated cells (control)}}$$

The IC_{50} value was determined as the concentration of the complexes that is required to reduce the absorbance to half that of the control.

***In vitro* antiproliferative Activity**

Cell culture and treatment

Human hepatoma cell line Huh7, was grown in Dulbecco's modified Eagle's medium (DMEM, Gibco–BRL) supplemented with 10% fetal bovine serum (FBS, Gibco–BRL) and 10 μg of gentamycin mL^{-1} at 37°C in 5% CO_2. In the treatment group, Huh7 cells treated for 48 h with test complexes **2** and **3**, at final concentration of 35 μM, along with vehicle control alone (DMSO).

Cell proliferation assay

Huh7 cells were plated in quadruplicate at a density of 60,000 cells/well in 2 mL of respective culture media in six well plates. Cells were grown in the regular medium with 5% FBS in the control and treated with complex. Cell growth curve was analyzed at dose of (35μM). Cells were trypsinized, and the number of viable cells was determined by 0.4% trypan blue and counted at different time points starting from day 0 to 48 h, using a Coulter Counter (Model ZF; Coulter Electronics, Hertfordshire, UK).

Quantitative real time RT–PCR

Total cellular RNA from control and treated (complexes **2** and **3**) Huh7 cells were extracted using Trizol (Invitrogen Life Technologies) according to manufacturer's protocol. Two micrograms of total RNA was used for reverse transcription for cDNA preparation. The cDNA was then used to quantify different genes by real time PCR (Applied Biosystem, 7500 Real Time PCR system). The primers used to quantify different genes are mentioned in Table 3.

Statistical analysis

Results were analyzed as the mean ±SEM, and comparisons of the experimental data were by two tailed independent sample student's *t*–test. *P* value of <0.05 was considered statistically significant.

Molecular docking

The rigid molecular docking studies were performed by using HEX 6.1 software,[67b] is an interactive molecular graphics program for calculating and displaying feasible docking modes of a pairs of protein, enzymes and DNA molecule. Structures of the complexes were sketched by CHEMSKETCH (http://www.acdlabs.com) and convert it into pdb format from mol format by OPENBABEL (http://www.vcclab.org/lab/babel/). The crystal structure of the B–DNA

dodecamer d(CGCGAATTCGCG)$_2$ (PDB ID: 1BNA) and human–DNA–topo I complex (PDB ID: 1SC7) were downloaded from the protein data bank (http://www.rcsb.org./pdb). All calculations were carried out on an Intel Pentium 4, 2.4 GHz based machine running MS Windows XP SP2 as operating system. Visualization of the docked pose has been done by using CHIMERA (www.cgl.ucsf.edu/chimera) and PyMol (http://pymol.sourceforget.net/) molecular graphics program.

Conclusion

Herein, we have designed and synthesized new organotin complexes **1**–**3** with an aim to explore their potential chemotherapeutic applicability as organotin(IV) complexes in cell biology offer diverse opportunities for manipulating biological processes. Initially, the binding behaviors of the complexes with CT DNA have been investigated using absorption and fluorescence spectroscopy, exhibited the strong binding of the complexes GSnEA (**2**) and MSnEA (**3**) to CT DNA via electrostatic interaction mode that preferentially involves the phosphodiester backbone. The artificial nuclease activity was ascertained by gel electrophoretic mobility assay; the complexes **2** and **3** displayed efficient cleavage activity of plasmid pBR322 DNA. Both the complexes displayed significantly good Topo I inhibition activity as compared with some standard drugs. Additionally, molecular docking studies were performed with molecular target DNA and the active site of Topo I enzyme, in order to validate the experimental results. Furthermore, both the complexes have been tested against a human hepatoma cancer cell line showed good antiproliferative activity and significantly inhibit the expression of MMP–2 mRNA levels. Thus, it emerges from the present study that the water–soluble carbohydrate–based organotin complexes can act as an efficacious antiproliferative drug by inducing morphological changes consistent with the induction of apoptotic cell death.

Acknowledgment

We express our gratitude to DBT, New Delhi, for generous financial support (Scheme no. BT/PR6345/MED/14/784/2005). Thanks to SAIF Chandigarh for elemental analysis, NMR, ESI MS and Mr Musheer Ahmad, Indian Institute of Technology, Kanpur for single crystal analysis. The authors acknowledge financial support to the Department of Chemistry, AMU through UGC assisted DRS–SAP and DST PURSE Programme.

Supporting Information

Crystallographic data are also available from the CCDC as file CCDC 969131.

References

1. G. Marks, W. K. Beatty, *The Precious Metals of Medicine, Charles Scribner's Sons*; New York (1975) pp. 294.
2. B. Rosenberg, L. VanCamp, J. E. Trosko, V. H. Mansour, *Nature* 1969, **222**, 385–386.
3. B. Rosenberg, *Interdiscip. Sci. Rev.* 1978, **3**, 134–147.
4. (a) M. Galanski, V. B. Arion, M. A. Jakupec, B. K. Keppler, *Curr. Pharm. Design* 2003, **9**, 2078–2089. (b) B. Rosenberg, *Adv. Exp. Med. Biol.* 1977, **91**, 129–150.(c) J. M. Hill, R. J. Speer, *Anticancer Res.* 1982, **2**, 173–186.
5. M. Galanski, M. A. Jakupec, B. K. Keppler, *Curr. Med. Chem.* 2005, **12**, 2075–2094.
6. C. G. Hartinger, P. J. Dyson, *Chem. Soc. Rev.* 2009, **38**, 391–401.
7. (a) K. Strohfeldt, M. Tacke, *Chem. Soc. Rev.* 2008, **37**, 1174–1187.(b) Dalton transactions themed issue on metal anticancer compounds, *Dalton Trans.* 2009, 10629–10936.
8. C. A. Vock, W. H. Ang, C. Scolaro, A. D. Phillips, L. Lagopoulos, L. Juillerat–Jeanneret, G. Sava, R. Scopelliti, P. J. Dyson, *J. Med. Chem.* 2007, **50**, 2166–2175.
9. (a) J. Maksomiska, D. S. Williams, G. E. Atilla–Gokcumen, K. S. M. Smalley, P.J. Carroll, R. D. Webster, P. Filippakopoulos, S. Knapp, M. Herlyn, E. Meggers, *Chem.–Eur. J.* 2008, **14**, 4816–4822. (b) W. H. Ang, L. J. Parker, A. De Luca, L. Juillerat–Jeanneret, C. J. Morton, M. Lo Bello, M. W. Parker, P. J. Dyson, *Angew. Chem. Int. Ed.* 2009, **48**, 3854–3857.
10. (a) N. Metzler–Nolte, *Angew. Chem. Int. Ed.* 2001, **40**, 1040–1043.(b) N. Metzler–Nolte, *Chimia* 2007, **61**, 736–741..
11. A. Alama, B. Tasso, F. Novelli, F. Sparatore, *Drug Discov. Today* 2009, **14**, 500–508.

12.(a) S. Tabassum, C. Pettinari, *J. Organomet. Chem.* 2006, **691**, 1761–1766. (b) P. J. Smith, A. J. Crow, R. Hill, *International Tin Research Institute*; London, 1979. (c)M. Gielen, E. R. T. Tiekink, *Metallotherapeutic drugs and metal based diagnostic agents. The use of Metals in Medicine*; J. Wiley & Sons (2005) pp. 421–439.

13. (a) L. Pellerito, L. Nagy, *Coord. Chem. Rev.* 2002, **224**, 111– 150 and references therein. (b) M. L. Falcioni, M. Pellei, R. Gabbianelli, *Mutat. Res.* 2008, **653**, 57–62 and references therein.(c) Q. Li, P. Yang, H. Wang, M. Guo, *J. Inorg. Biochem.* 1996, **64**, 181 –195.(d) J. S. Casas, E. E. Castellano, M. D. Couce, J. Ellena, A. Sanchez, J. L. Sanchez, J. Sordo, C. Taboada, *Inorg. Chem.* 2004, **43**, 1957 – 1963.(e) Y. Arakawa, *Biomed. Res. Trace Elem.* 2000, **11**, 259– 286.

14. (a) C. Syng-Ai, T. S. Basu Baul, A. Chatterijee, *J. Environ. Pathol. Toxicol. Oncol.* 2001, **20**, 333 –342.(b) F. Barbieri, M. Viale, F. Sparatore, G. Schettini, A. Favre, C. Bruzzo, F. Novelli, A. Alema, *Anticancer Drugs* 2002, **13**, 599– 604.(c) H. Seibert, S. Moerchel, M. Guelden, *Cell. Biol. Toxicol.* 2004, **20**, 273 –283.(d) N. Hcti, J. Ma, S. Tabassum, Y. Wang, M. Wu, *J. Biochem.* 2003, **134**, 521 –528.

15. L. Rocamora-Reverte, E. Carrasco-Garcia, J. Ceballos-Torres, S. Prashar, G. N. Kaluderovic, J. A. Ferragut, S. Gomez-Ruiz, *ChemMedChem* 2012, **7**, 301 – 310.

16. (a) T. Storr, K. H. Thompson, C. Orvig, *Chem. Soc. Rev.* 2006, **35**, 534–544.(b) W. H. Ang, P. J. Dyson, *Eur. J. Inorg. Chem.* 2006, **20**, 4003–4018.

17. C. G. Hartinger, A. A. Nazarov, S. M. Ashraf, P. J. Dyson, B. K. Keppler, *Curr. Med. Chem.* 2008, **15**, 2574–2591.

18. S. Hanessian, (*Ed.) Preparative Carbohydrate Chemistry, Marcel Dekker Inc.*; New York (1986) pp. 650.

19. P. Nangia–Makker, J. Conklin, V. Hogan, A. Raz, *Trends Mol. Med.* 2002, **8**, 187–192.

20. F. Morel, M. Renoux, P. Lachaume, S. Alziari, *Mutat. Res.* 2008, **637**, 111–117.

21. E. G. Chiorean, T. Dragovich, J. Hamm, V. K. Langmuir, S. Kroll, D. T. Jung, A. B. Colowick, G. F. Tidmarsh, P. J. Loehrer, *Cancer Chemother. Pharmacol.* 2008, **61**, 1019–1026.

22. F. A. Fornari, J. K. Randolph, J. C. Yalowich, M. K. Ritke, D. A. Gewirtz, *Mol. Pharmacol.* 1994, **45**, 649–656.

23. S. Tabassum, S. Mathur, F. Arjmand, K. Mishra, K. Banerjee, *Metallomics* 2012, **4**, 205–217.

24. S. Yano, S. Inoue, Y. Yasuda, T. Tanase, Y. Mikata, T. Kakuchi, T. Tsubomura, M. Yamasaki, I. Kinoshita M. Doe, *J. Chem. Soc., Dalton Trans.* 1999, 1851–1856.

25. (a) Z. Shi, S. Tabassum, W. Jiang, J. Zhang, S. Mathur, J. Wu, Y. Shi, *ChemBioChem,* 2007, **8**, 2092–2099. (b) R. P. Bhandwar, C. P. Rao, *Carbohydr. Res.* 1996, **287**, 157–168.

26. A. Szorcsik, L. Nagy, L. Pellerito, T. Yamaguchi, K. Yoshida, *J. Radioanal. Nucl. Chem.* 2003, **256**, 3–10.

27. T. P. Lockhart, W. F. Manders, *Inorg. Chem.* 1986, **25**, 892–895.

28. K. Ishida, S. Nonoyama, T. Hirano, S. Yano, M. Hidai, S. Yoshikawa, *J. Am. Chem. Soc.* 1989, **111**, 1599–1604.

29. V. Barba, E. Vega, R. Luna, H. Hopfl, H. I. Beltran, L. S. Z. Rivera, *J. Organomet. Chem.* 2007, **692**, 731–739.

30. C. N. N'soukpoe Kossi, C. Descoteaux, E. Asselin, H. A. T. Riahi, G. Be´rube, *DNA and Cell Biol.* 2008, **27**, 101–107.

31. (a) S. Walker, K. G. Valentine, D. Kahne, *J. Am. Chem. Soc.* 1990, **112**, 6428–6429.(b) W. Ding, G. A. Ellestad, *J. Am. Chem. Soc.,* 1991, **113**, 6617. (c) M. Uesugi, Y. Sugiura, *Biochemistry,* 1993, **32**, 4622–4627.

32. S. Tabassum, R. A. Khan, F. Arjmand, M. Aziz, A. S. Juvekar, S. M. Zingde, *Carbohydr. Res.* 2011, **346**, 2886–2895.

33. J. W. Lown, *Anthracycline and Anthracenedione–based Anticancer Agents*; Elsevier, New York (**1988**).

34. J. Rojo, J.C. Morales, S. Penadés, *Topics in Current Chemistry*; Springer –Verlag, Berlin Heidelberg (2002) vol. 218, 45–92.

35. A. Wolfe, G. H. Shimer, T. Meehan, *Biochemistry* 1987, **26**, 6392–6396.

36. C. Tong, Z. Hu, W. Liu, *J. Agric. Food Chem.* 2005, **53**, 6207–6212.

37. G. Han, P. Yang, *J. Inorg. Biochem.* 2002, **91**, 230–236.

38. Q. Li, P. Yang, H. Wang M. Guo, *J. Inorg. Biochem.* 1996, **64**, 181–195.

39. Q. H. Zhou, P. Yang, *Chin. J. Chem.* 2005, **23**, 521–524.

40. J. A. Cowan, *Curr. Opin. Chem. Biol.* 2001, **5**, 634–642.

41. A. Sreedhara, J. A. Cowan, *J. Biol. Inorg. Chem.* 2001, **6**, 337–347.

42. J. Chen, X. Wang, Y. Shao, J. Zhu, Y. Zhu, Y. Li, Q. Xu, Z. Guo, *Inorg. Chem.* 2007, **46**, 3306–3312.

43. A. K. Larsen, A. E. Escargueil, A. Skladanowski, *Pharmacol. Ther.* 2003, **99**, 167−181.

44. L. F. Liu, *Annu. Rev. Biochem.* 1989, **58**, 351−375.

45. J. A. Holden, *Curr. Med. Chem. Anti –Cancer Agents,* 2001, **1**, 1−25.

46. J. J. Champoux, *Annu. Rev. Biochem.* 2001, **70**, 369−413.

47. K. Suzuki, M. Uyeda, *Biosci. Biotechnol. Biochem.* 2002, **66**, 1706–1712.

48. K. Suzuki, F. Shono, M. Uyeda, *Biosci. Biotechnol. Biochem.* 1998, **62**, 2073–2075.

49. K. Bielawski, A. Bielawski, T. Anchim, S. Wolczynski, *Biol. Pharm. Bull.* 2005, **28**, 1004–1009.

50. E. Trotta, N. Del Grosso, M. Erba, M. Paci, *Biochemistry* 2000, **39**, 6799–6808.

51. L. A. Liotta, W. G. Stetler–Stevenson, *Cancer Res.* 1991, **51**, 5054–5059.

52. T. Oshima, C. Kunisaki, K. Yoshihara, R. Yamada, N. Yamamoto, T. Sato, *Oncol. Rep.* 2008, **19**, 1285–1291.

53. L. Hao, C. Zhang, Y. Qiu, L. Wang, Y. Luo, M. Jin, Y. Zhang, T. B. Guo, K. Matsushima, Y. Zhang, *Cancer Lett.* 2007, **253**, 34–42.

54. (a) S. Sillanpää, M. Anttila, K. Voutilainen, K. Ropponen, T. Turpeenniemi–Hujanen, U. Puistola, R. Tammi, M. Tammi, R. Sironen, S. Saarikoski, V. M. Kosma, *Gynecol. Oncol.* 2007, **104**, 296–303. (b) R. L. Elliott, G. C. Blobe, *J. Clin. Oncol.* 2005, **23**, 2078–2093.

55. (a) A. Nawshad, D. Lagamba, A. Polad, E. D. Hay, *Cells Tissues Organs* 2005, **179**, 11–23.(b) S. Xie, P. Macedo, M. Hew, C. Nassenstein, K. Y. Lee, K. F. Chung, *Respir. Res.* 2009, **22**, 10–40.

56. R. Rohs, I. Bloch, H. Sklenar, Z. Shakked, *Nucl. Acids Res.* 2005, **33**, 7048–7057.

57. L. F. De Castro, M. Zacharias, *J. Mol. Recognit.* 2002, **15**, 209–220.

58. X. Xiao, S. Antony, Y. Pommier, M. Cushman, *J. Med. Chem.* 2005, **48**, 3231–3238.

59. H. T. M. Van, W. –J. Cho, *Bioorg. Med. Chem. Lett*. 2009, **19**, 2551–2554.

60. Siemens, SMART and SAINT, Area Detector Control and Integration Software, Siemens Analytical X–Ray Systems, Inc., Madison, Wisconsin, USA, 1996.

61. Siemens, SHELXTL, Version 5 Reference Manual, Siemens Analytical X–ray Systems, Inc., Madison, Wisconsin, USA, 1996.

62. G. M. Sheldrick, *Acta Crystallogr., Sect. A: Found. Crystallogr.* 2008, A64, 112–122; *Program for Crystal Structure Solution and Refinement, University of Goettingen, Germany,* 1997.

63. L. J. Farrugia, *J. Appl. Crystallogr.* 1997, **30**, 565.

64. M. E. Reichmann, S. A. Rice, C. A. Thomas, P. Doty, *J. Am. Chem. Soc.* 1954, **76**, 3047 –3053.

65. J. R. Lakowicz, G. Weber, *Biochemistry* 1973, **12**, 4161 –4170.

66. (a) F. Arjmand, F. Sayeed, S. Parveen, S. Tabassum, A. S. Juvekar, S. M. Zingde, *Dalton Trans.* 2013, **42**, 3390–3401.(b) S. Tabassum, W. M. Al–Asbahy, M. Afzal, F. Arjmand, V. Bagchi*, Dalton Trans.* 2012, **41**, 4955–4964. (d) Sartaj Tabassum, Mehvash Zaki, Mohd. Afzal and Farukh Arjmand *Dalton Trans.*, 2013,**42**, 10029-10041. (d) M. Chauhan, K. Banerjee, F. Arjmand, *Inorg. Chem.* 2007, **46**, 3072–3082.(e) R. A. Khan, A. Ahmad, R. Kakkar, D. Gupta, V. Bagchi, S. Tabassum, *Organometallics,* 2013, **32**, 2546-2551.

Table 1: Crystal data and structure refinement parameters for **SnEA** complex.

Compound	**SnEA (1)**
CCDC No.	969131
Empirical formula	$C_6H_{20}Cl_2N_2O_2Sn$
Formula weight	341.85
T (K)	100 K
ʎ (Å)	0.71073 Å
μ (mm^{-1})	2.01
Crystal system	Monoclinic
Space group	*Cc*
a (Å)	17.228 (3)
b (Å)	8.8924 (13)
c (Å)	12.8756 (19)
β (º)	129.374 (2)°
V ($Å^3$)	1524.8 (4)
Z	4
D_{calc} (mg/m^3)	1.489
Radiation type k (Å)	Mo Kα
F(0 0 0)	680
Crystal size (mm)	0.27 × 0.19 × 0.15
Crystal colour, shape	colourless, block
Scan range θ (º)	2.8–26.1
Index ranges	–20 ≤ h ≤ 21
	–10 ≤ k ≤ 10
	–15 ≤ l ≤ 15
No. measured reflections	4081
No. independent reflections	2118
R_{int}	0.018
No. refined parameters	143
No. observed reflections, I ≥ 2σ (I)	1997
Goodness –of –fit on F^2, S	1.14
$R[F^2 > 2\sigma(F^2)]$, $wR(F^2)$	0.046, 0.151
max, min electron density ($eÅ^{-3}$)	1017, –0.74

Table 2: Inhibitory effects on topoisomerases Iα of complex **2** and **3** and some reported Topo I Inhibitors**.**

Drug	**Inhibitory activity (IC_{50})**
	Topo I (μM)
Camptothecin	17
Novobiocin	>100
Etoposide	>1000
Hoechst 33258	30
Complex **2**	20 (This work)
Complex **3**	30 (This work)

Table 3: Primer sequence and annealing temperatures used for real time PCR.

Primer Name	**Primer sequence**	**Annealing (°C)**	**References**
MMP –2	CCCTCCCTTCAACCATTCCC TTCCAGCAGACACCATCACC	55	Oshima *et al.,* 2008
TGF –β	CAAGGACCTCGGCTGGAA CCGGGTTATGCTGGTTGTACA	58	Xie *et al.*, 2009
GAPDH	CGACCACTTTGTCAAGCTCA AGGGGTCTACATGGCAACTG	55 –60	

Figure captions

Figure 1. ORTEP view (50% probability level) of structure of the complex SnEA (**1**), drawing of ORTEP view was done using PLATON software.

Figure 2. Absorption spectra of (a) complex **2** and (b) complex **3** in Tris–HCl buffer (pH= 7.2) in the absence and presence of increasing amounts of CT DNA. Arrows indicate the increase in the intensity upon increasing DNA concentration.

Figure 3. Emission spectra of (**a**) complex **2** and (**b**) complex **3** in Tris–HCl buffer (pH 7.2) in the absence and presence of CT DNA. Arrows indicate the change in the intensity upon increasing DNA concentration

Figure 4. Effect of increasing concentration of K_2HPO_4 on the fluorescence intensity of (**a**) complex **2** and (**b**) complex **3** M=(10^{-3} M) with DNA (10^{-4} M).

Figure 5. Effect of different concentration of NaCl on the fluorescence spectra of (a) complex **2** and (b) complex **3** with CT DNA (10^{-4}M). Arrows indicate the gradual decrease of emission intensity as a function of NaCl concentration.

Figure 6. Agarose gel electrophoresis patterns for the cleavage of pBR322 plasmid DNA as a function of increasing concentration of complex **(a)** complex **2,** Lane 1: DNA control, Lane 2: DNA + 10μM of **2**, Lane 3: DNA + 20μM of **2**, Lane 4: DNA + 30μM of **2**, Lane 5: DNA + 40μM of **2**, Lane 6: DNA + 50μM of **2**. **(b)** complex **3**, Lane 1: DNA control, Lane 2: DNA + 10μM of **3**, Lane 3: DNA + 20μM of **3**, Lane 4: DNA + 30μM of **3**, Lane 5: DNA + 40μM of **3**, Lane 6: DNA + 50μM of **3**.

Figure 7. Inhibitory effect of the complex on human topoisomerases Iα. Agarose gel electrophoresis patterns showing the effect of different concentrations of complex on the activity of DNA–Topo Iα (Topo I); **(a)** complex **2,** Lane 1, DNA control; Lane 2, Topo I + DNA; Lane

3, 20 μM of **2** + DNA + Topo I; Lane 4: 30 μM of **2** + DNA + Topo I; Lane 5: 40 μM of **2** + DNA + Topo I. **(b)** complex **3,** Lane 1, DNA control; Lane 2, Topo I + DNA; Lane 3, 20 μM of **3** + DNA + Topo I; Lane 4: 30 μM of **3** + DNA + Topo I; Lane 5: 40 μM of **3** + DNA + Topo I.

Figure 8. Cell viability of complexes **2** and **3** on Huh7 cancer cell line. Each data point is the mean standard error obtained from at least three independent experiments.

Figure 9. Effect of complex **2** and **3** on the proliferation of Huh7 cells. Huh7 cells were seeded at the same density a day before treatment. Next day the cells were subjected treatment with an optimized concentration of **2**, **3** and vehicle control alone (DMSO) in a six well plate. The antiproliferative effect of these compounds was measured microscopically at different time intervals and also by growth curve analysis. At each time point (24 and 48h), cells were trypsinized and counted as described in Materials and Methods section. All data presented are expressed as mean ±SEM of triplicate wells for each time point. Significant difference from the control is represented by an asterisk (P<0.05).

Figure 10. Effect of complex **2** and **3** on the expression of tumor promoting and suppressor gene. RNA from control and treatment groups was analyzed for the expression of genes (**a**) MMP–2 and (**b**) TGF–β by real time PCR. Changes in the mRNA expression of the respective genes were determined as relative mRNA expression against internal control GAPDH. The experiment was repeated thrice and significant difference from the control is represented by an asterisk (P<0.05).

Figure 11. Molecular docked model of complex (**a**) **2** and (**b**) **3** with DNA [dodecamer duplex of sequence d(CGCGAATTCGCG)$_2$ (PDB ID: 1BNA)].

Figure 12. Diagram showing in molecular docked model of complex (a) **2** and (b) **3** in the cleavage active site of human DNA Topo I (PDB ID: 1SC7).

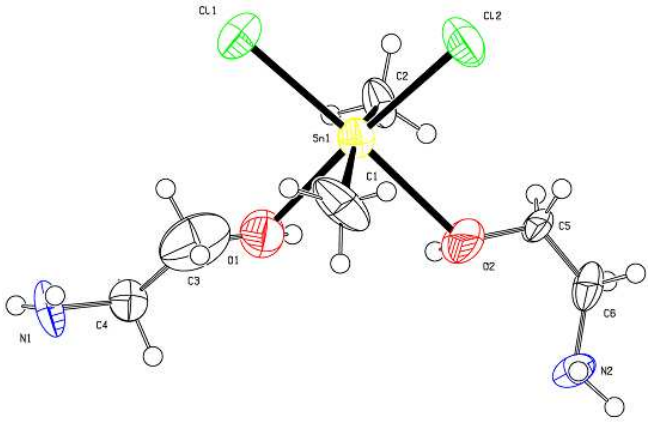

Figure 1.

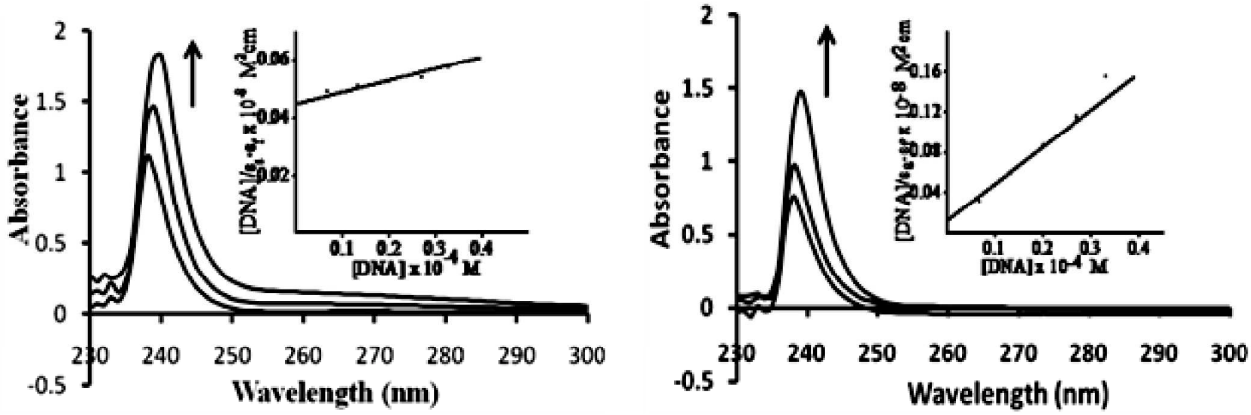

(a) **(b)**

Figure 2.

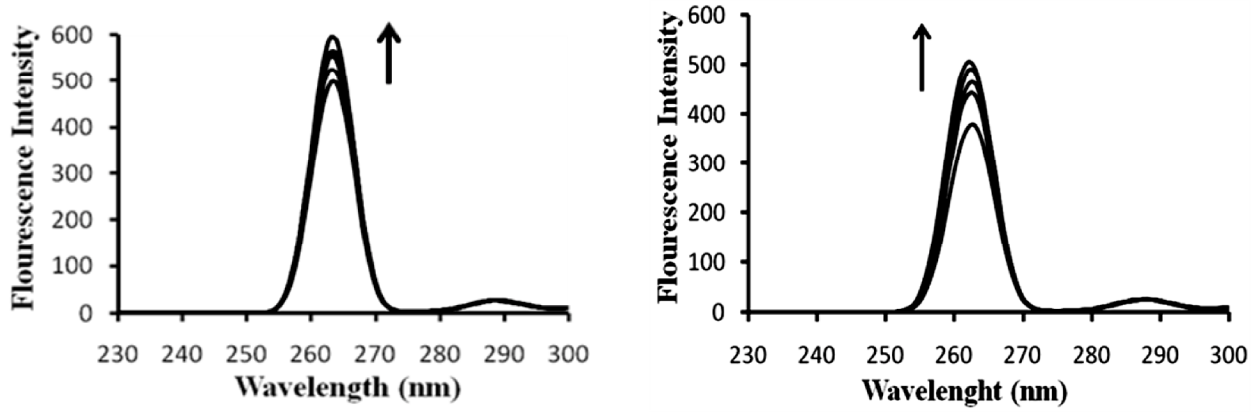

(a) **(b)**

Figure 3.

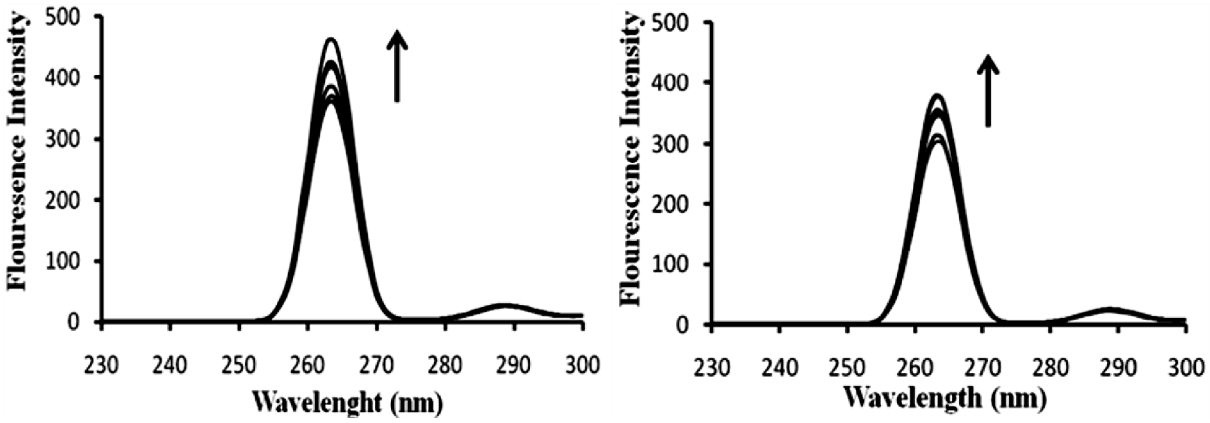

(a) (b)

Figure 4.

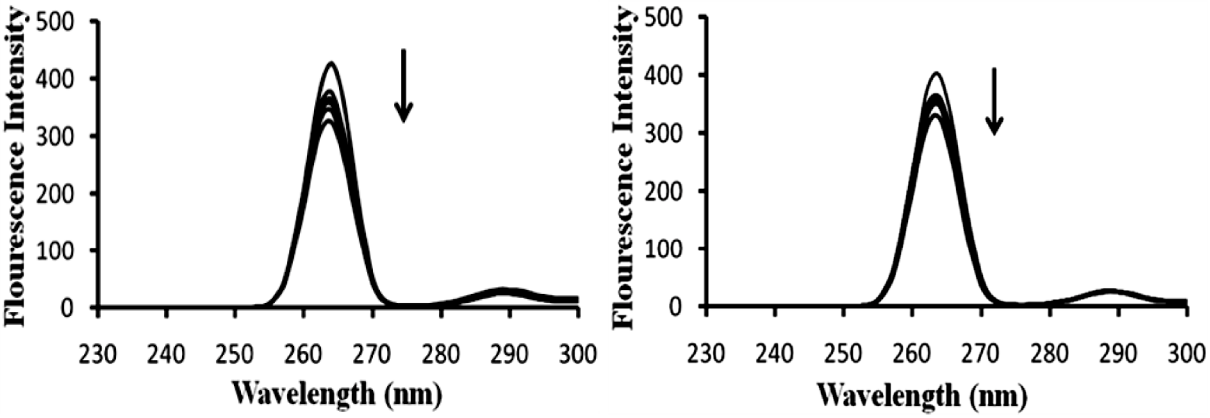

(a) (b)

Figure 5.

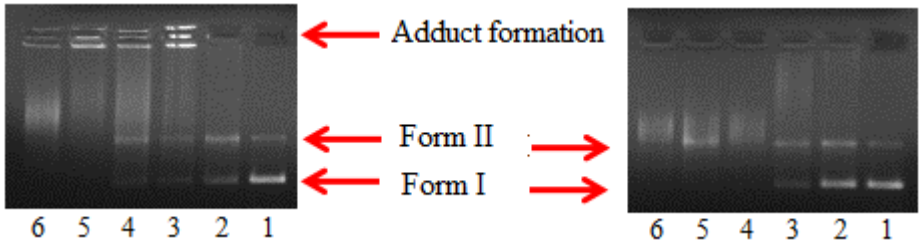

(a) (b)

Figure 6.

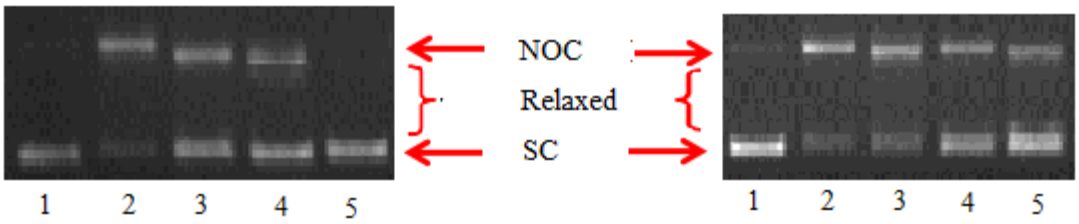

(a) (b)

Figure 7.

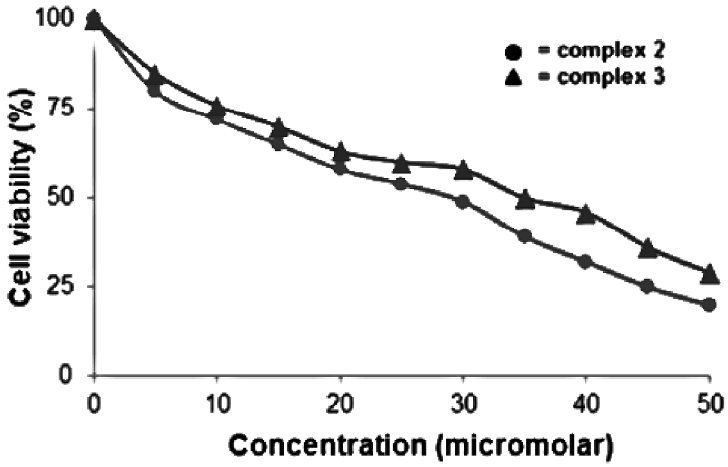

Figure 8.

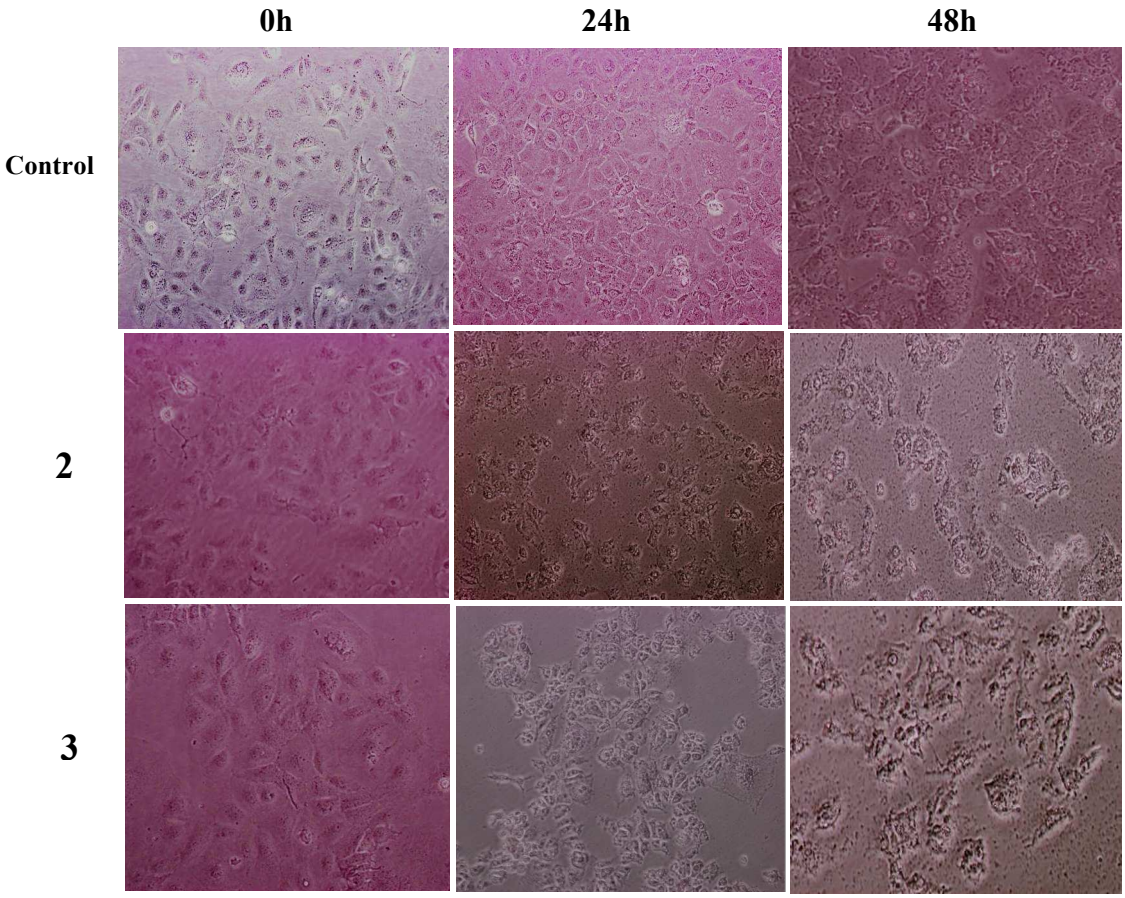

(a)

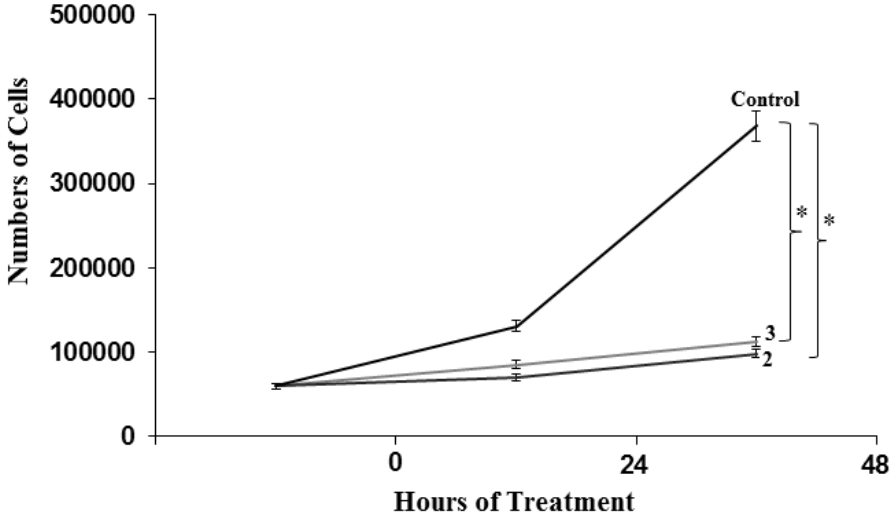

(b)

Figure 9.

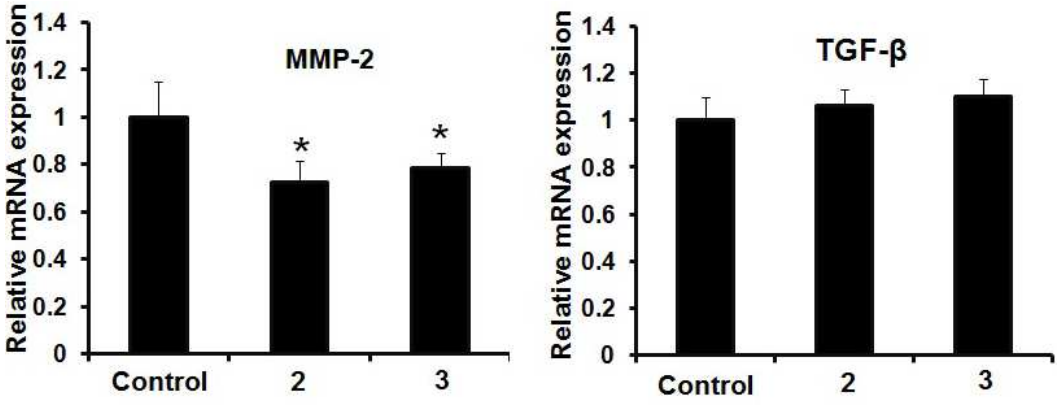

(a) **(b)**

Figure 10.

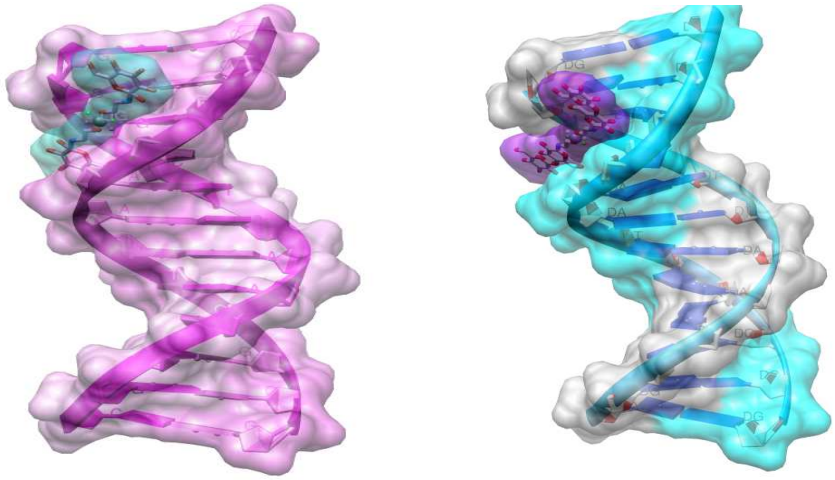

(a) **(b)**

Figure 11.

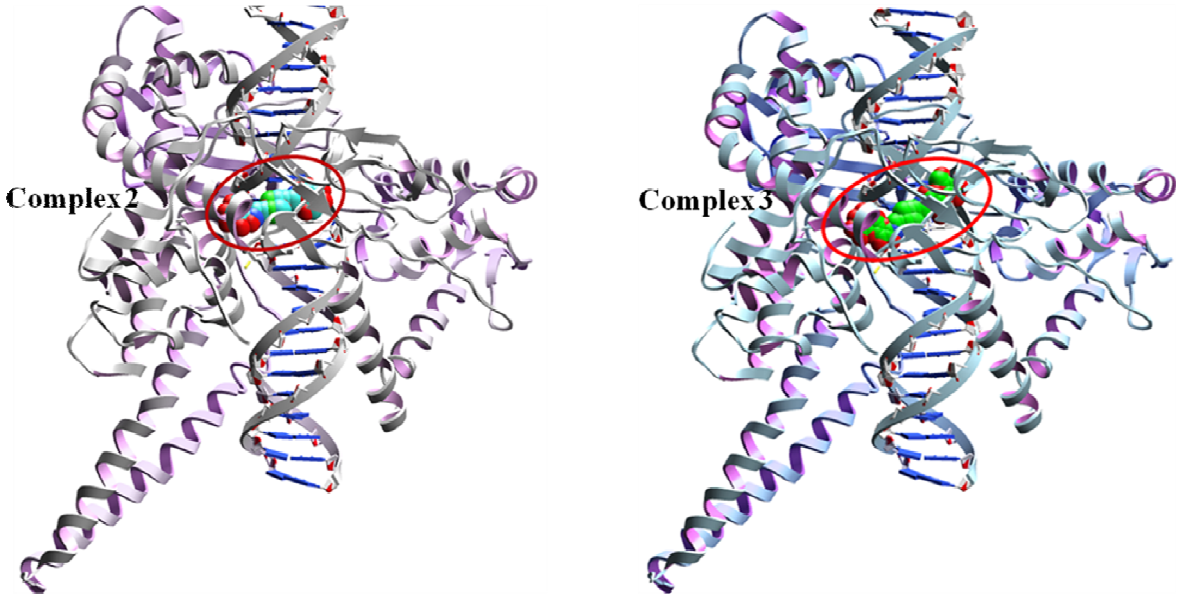

(a) (b)

Figure 12.

Scheme 1. Synthesis of Complexes 1–3.

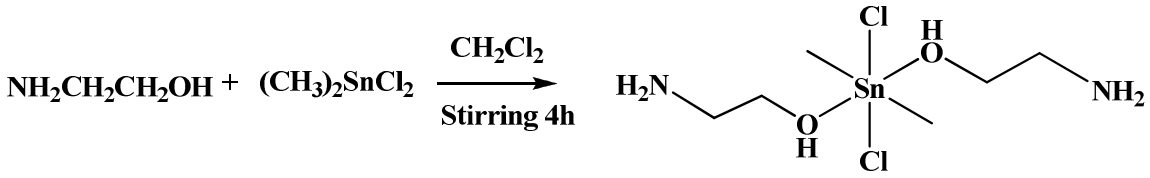

SnEA (1)

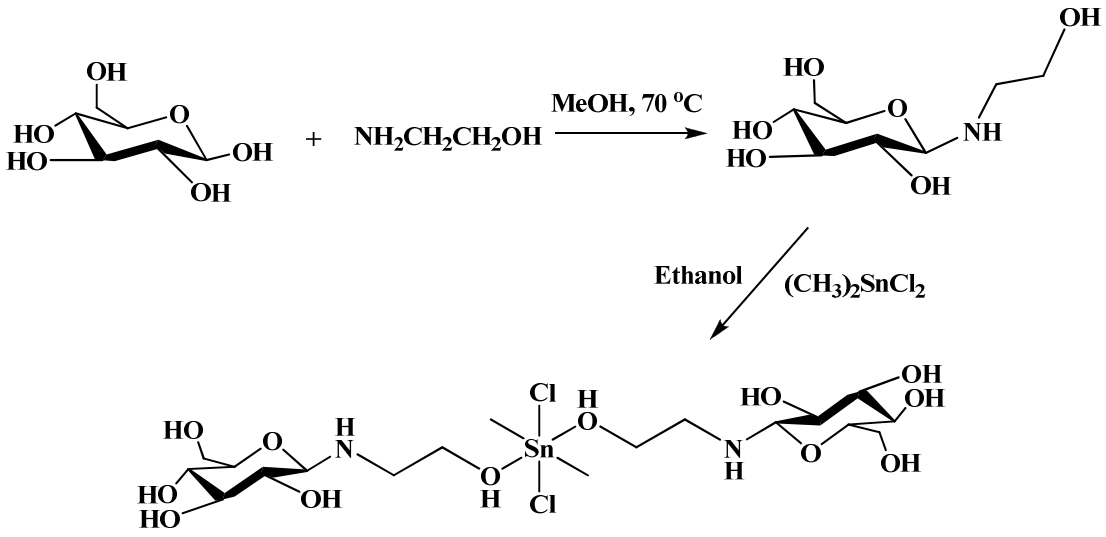

GSnEA (2)

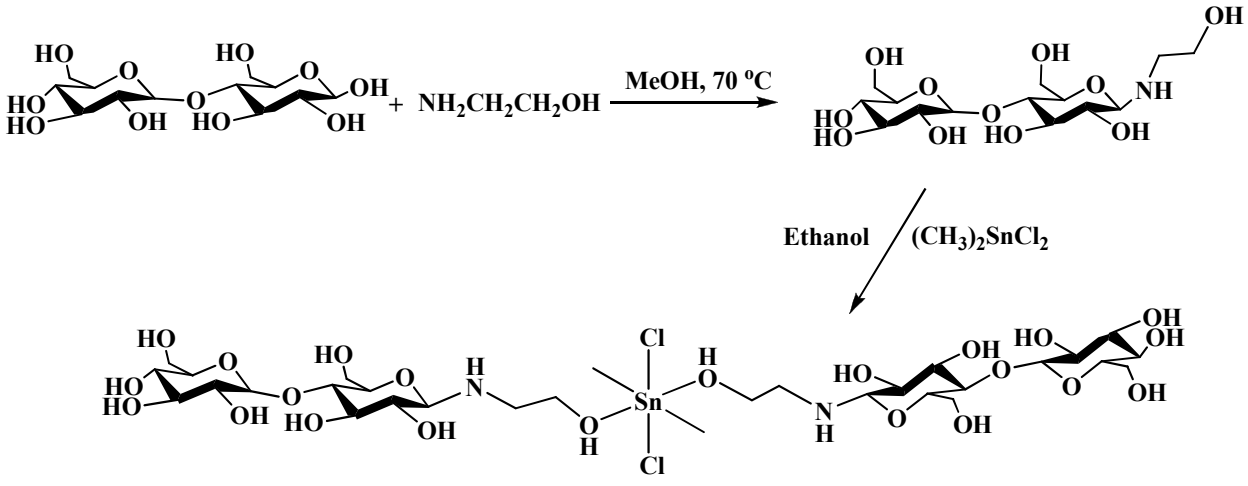

MSnEA (3)

Carbohydrate Linked Organotin(IV) Complexes as Human Topoisomerase Iα Inhibitor and their Antiproliferative Effects Against Human Carcinoma Cell Line

Rais Ahmad Khan[a], Shipra Yadav [a], Zahid Hussain [b], Farukh Arjmand[a] and Sartaj Tabassum.[a]*

[a*] *Department of Chemistry, Aligarh Muslim University, Aligarh –202002, India.*

[b] *Centre of Excellence in Biotechnology Research, KSU, Riyadh, KSA.*

Graphical Abstract